Spinal Subarachnoid Space Pressure Measurements in an In Vitro Spinal Stenosis Model: Implications on Syringomyelia Theories

Bryn A. Martin[1]
Integrative Bioscience Institute,
Laboratory of Hemodynamics and Cardiovascular Technology,
École Polytechnique Fédérale de Lausanne,
Lausanne 1015, Switzerland
e-mail: brynandrew.martin@epfl.ch

Richard Labuda
Chiari and Syringomyelia Patient Education Foundation,
Wexford, PA 15090

Thomas J. Royston
Department of Mechanical and Industrial Engineering,
University of Illinois at Chicago,
Chicago, IL 60607

John N. Oshinski
Department of Radiology and Biomedical Engineering,
Emory University,
Atlanta, GA 30322

Bermans Iskandar
Department of Neurological Surgery,
University of Wisconsin Medical School,
Madison, WI 53792

Francis Loth
Departments of Mechanical and Biomedical Engineering,
University of Akron,
Akron, OH 44325

Full explanation for the pathogenesis of syringomyelia (SM), a neuropathology characterized by the formation of a cystic cavity (syrinx) in the spinal cord (SC), has not yet been provided. It has been hypothesized that abnormal cerebrospinal fluid (CSF) pressure, caused by subarachnoid space (SAS) flow blockage (stenosis), is an underlying cause of syrinx formation and subsequent pain in the patient. However, paucity in detailed in vivo pressure data has made theoretical explanations for the syrinx difficult to reconcile. In order to understand the complex pressure environment, four simplified in vitro models were constructed to have anatomical similarities with post-traumatic SM and Chiari malformation related SM. Experimental geometry and properties were based on in vivo data and incorporated pertinent elements such as a realistic CSF flow waveform, spinal stenosis, syrinx, flexible SC, and flexible spinal column. The presence of a spinal stenosis in the SAS caused peak-to-peak cerebrospinal fluid CSF pressure fluctuations to increase rostral to the stenosis. Pressure with both stenosis and syrinx present was complex. Overall, the interaction of the syrinx and stenosis resulted in a diastolic valve mechanism and rostral tensioning of the SC. In all experiments, the blockage was shown to increase and dissociate SAS pressure, while the axial pressure distribution in the syrinx remained uniform. These results highlight the importance of the properties of the SC and spinal SAS, such as compliance and permeability, and provide data for comparison with computational models. Further research examining the influence of stenosis size and location, and the importance of tissue properties, is warranted.
[DOI: 10.1115/1.4000089]

Keywords: cerebrospinal fluid hydrodynamics, syringomyelia, Chiari malformation, hydrocephalus, fluid-structure interaction, spinal cord, subarachnoid space stenosis, syrinx, intracranial and spinal pressures, in vitro model

1 Introduction

Many theories have been developed to provide an explanation for the pathogenesis of syringomyelia (SM), nearly all of which place significant emphasis on the pressure environment within the spinal subarachnoid space (SAS). It has been postulated that an abnormal pressure environment caused by a cerebrospinal fluid (CSF) flow blockage in the SAS leads to syrinx pathogenesis and subsequent pain in the patient. However, paucity and lack of detail in spinal SAS pressure measurements have left researchers with little evidence to scrutinize the existing SM theories.

1.1 Pressure Measurements. Pressure measurements in the spinal SAS with CSF flow blockage have been obtained in vivo in patients and animal models and by computational and laboratory bench-top experiments. Heiss et al. measured intracranial pressure (ICP), cervical and lumbar SAS pressure in patients with SM [1]. Williams also measured longitudinal pressure dissociation (LPD) in the spinal SAS of patients [2–5]. Milhorat et al. measured intramedullary fluid pressure in patients undergoing syrinx shunting procedures [6]. In vivo pressure measurements in the SAS with post-traumatic syringomyelia (PTS) have been obtained in dogs by Williams [7], Williams and Bentley [8], and Hall et al. [9], in sheep by Stoodley et al. [10], and in cats by Klekamp et al. [11]. An in vitro study by Martin et al. documented CSF flow, pressure, and spinal cord (SC) motion in a SM experiment without a spinal stenosis [12]. Pressure calculations have been documented in computational models of SM by Carpenter and co-workers [13,14], Bertram et al. [15,16], and Bilston et al. [17]. Longitudinal pressure variation in a healthy spinal SAS was calculated by Loth et al. [18]. Chang and Nakagawa looked at pressure distribution in an electrical circuit equivalent model of the CSF system [19]. A model for noninvasive measurement of ICP was developed by Alperin et al. [20].

The presented studies have quantified the pressure environment in the SAS with SM. However, pressure is a highly complex parameter that can be examined in many ways including the temporal variation during the cardiac cycle as well as spatial gradients (lateral-ventral, rostral-caudal, and transmural across tissues). Pressure gradients are likely the driving force behind fluid motion in the SAS, into or out of the syrinx cavity, bulk motion of the SC, and stretching or compression of the SC parenchyma. Thus, a detailed examination of the pressure environment is warranted.

1.2 Syringomyelia Hypotheses. Hypotheses explaining the pathological mechanisms responsible for SM formation and/or progression have been made by many researchers, the majority

[1]Corresponding author.

Contributed by the Bioengineering Division of ASME for publication in the JOURNAL OF BIOMECHANICAL ENGINEERING. Manuscript received January 8, 2009; final manuscript received June 12, 2009; accepted manuscript posted September 1, 2009; published online October 20, 2010. Editor: Michael Sacks.

placing a significant role on abnormal craniospinal hydrodynamics due to obstructed CSF flow. The earliest hydrodynamic hypothesis based explanation for SM was given by Gardner and Angel in 1958 [21] and Gardner [22]. Gardner hypothesized that in Chiari malformation (CM) patients, the syrinx communicated freely with the fourth ventricle and that its enlargement was rooted in altered stresses in the hindbrain region. It has since been determined that the syrinx cavity often does not communicate freely with the fourth ventricle.

Williams proposed the "suck and slosh" theory to explain syrinx pathogenesis. This theory explained that CSF flows more easily (less resistance) in the caudocranial direction during coughing and/or valsalva, but not as easily in the craniocaudal direction [2], and that this was caused by a "ball-valve effect at the foramen magnum" [13,23]. This ball-valve effect would then cause LPD in the spinal SAS. To test this hypothesis, Williams [2–5,7], Williams and Bentley [8], and Williams [24] conducted experiments obtaining pressure measurements throughout the CSF system on both humans and animals. He suspected that pressure gradients could be exaggerated by enlargement of the syrinx, explaining the observation that larger diameter syrinxes progress faster than smaller ones [3,4] and the possibility that the size of the syrinx could be related to the CSF pulsation [25,26]. Williams was successful in providing evidence for LPD due to flow obstruction. This evidence was not sufficient to explain bulk movement of fluid into the syrinx but did help explain a mechanism to produce movement of fluid within the cavity.

Ball and Dayan proposed in 1972 that CSF could be forced though the Virchow–Robin spaces into the SC forming a cyst [27]. They observed a common histological feature in excised SCs in that they all had dilated perivascular spaces and suggested that a syrinx could form due to prolonged increased pressure in the CSF system caused by flow obstruction. Since Ball and Dayan's theory presentation, communication between the CSF and extracellular fluid has been supported in a number of studies [28–30].

Oldfield et al. developed a "systolic pressure theory" for the progression of a syrinx in patients with CM [31]. Oldfield et al. suggested that brain expansion during systole causes a CSF pressure wave to travel down the SAS across the foramen magnum. If this pressure wave was obstructed at the foramen magnum, the lower cerebellar tonsils could act with a pistonlike mechanism, resulting in impaction at the posterior region. The pistonlike action could then result in CSF movement through the perivascular spaces or dorsal root entry zone. Oldfield et al. provided evidence for the piston action of the tonsils by conducting research that recorded tonsillar movement during intra-operative ultrasound [27]. These measurements were successful in identifying a possible mechanism for damage to the SC due to the piston effect but did not provide pressure evidence to explain CSF movement through the cord tissue and into the syrinx.

Greitz proposed that a localized increase in CSF pulse pressure in the vicinity of a SAS obstruction, present in CM and most cases of PTS, causes accumulation of fluid in the distended SC [32]. He hypothesized that the Venturi effect could account for outward mechanical distension of the SC resulting in a suction effect on the surface of the cord and that the synergistic result of the flow obstruction and localized pressure drop would result in accumulation of extracellular fluid in the cord. Greitz suggested that the dilated caudal section of the syrinx indicated a decrease in CSF pressure in the adjacent SAS region and was supported by the observation that dilation only persisted when systolic CSF flow in the nearby SAS was present [1,31]. While the Venturi effect did provide a transient pressure gradient to expand the SC tissue locally, the theory lacked experimental evidence and did not explain the clinical observation of an elevated mean syrinx pressure [9].

Brodbelt et al. proposed that a syrinx could form if the normal flow of CSF through the perivascular spaces was disrupted by perturbations such as an arachnoid cyst, CM, SC tethering, or loss of compliance [33], and Stoodley proposed that all cystic cavities in the SC, whether canalicular or extracanalicular, are produced from this mechanism [34]. Stoodley et al. [10,30,37,38] and Brodbelt et al. [33,35,36] conducted many in vivo experiments to examine the movement of extracellular fluid into the SC and the central canal [39], showing in one study that more than a quarter of the patients with SC injury develop SM [40]. It has also been shown that the amount of trauma experienced by the SC is related to the extent of edema [41]. Brodbelt and Stoodley suggested that the pooling of CSF in the syrinx is likely caused by an imbalance of CSF flow moving into and out of the cyst [40] but that a passive mechanism for CSF transport into the SC did not explain the observation of a higher syrinx pressure than a SAS pressure [1,6,42].

A theoretical model was developed by Brodbelt et al. [33] and Bilston et al. [43] to examine the influence that the relative phase of arterial and CSF pulsations could have on fluid flow in the perivascular spaces. In this model, arterial pulsations were found to provide an active mechanism causing perivascular flow into the SC even with adverse pressure gradients of a few kilopascals [33]. This model was important in that it provided a possible fluid conduit, identified a valvelike transport mechanism, and was supported by in vivo and in vitro studies. However, Greitz contended that the dye tracer injection studies of Stoodley et al. did not prove bulk fluid motion but rather diffusion of fluid into the syrinx cavity without a preferred direction [32].

Levine proposed the venous congestion theory [44], which explained that the foramen magnum is obstructed in CM, causing higher CSF pulsations to occur above the blockage. Levine cited that CSF pressure in the SAS is regulated by the venous pressure during diastole and the arterial pressure during systole and that the amount of CSF moving into the extracellular spaces is related to the CSF flow waveform [11,37,45]. Flow obstruction at the foramen magnum results in the veins collapsing above the blockage and increasing in diameter below the blockage. Levine explained that this mechanism results in venous congestion and eventually leads to the formation of a syrinx. However, Perrin and Fehlings critiqued Levine because the venous congestion theory lacked experimental proof [46]. Iskandar et al. documented five cases of SM due to Chiari-like pathological conditions, which were lacking in hindbrain herniation yet responded favorably to traditional posterior fossa decompression surgery [47]. The implications of these relatively uncommon cases in terms of current theories are not entirely clear, but they do suggest that CSF flow obstruction due to a tight posterior fossa may be sufficient to cause a syrinx, even absent tonsillar herniation.

Computational models of fluid-filled coaxial elastic tube systems similar to that present in SM have been developed by Carpenter et al. [13], Berkouk et al. [14], Bertram et al. [15,16], Cirovic [48], and Cirovic et al. [49]. Carpenter identified that an "elastic jump" might account for transient rises in SAS pressure near a spinal stenosis site, but this concept was later disputed by Elliott et al. [50]. An electrical circuit equivalence model was developed by Chang and Nakagawa [19]. Bilston et al. developed a computational model of arachnoiditis in PTS modeled as a porous obstruction in the SAS and found that peak pressures in the SAS were strongly dependent on obstruction permeability [51]. Loth et al. performed hydrodynamic modeling of the pulsatile CSF flow in the spinal SAS [18]. In general, the computational models have been helpful to detail the spatial pressure environment but have employed significant assumptions such as axisymmetric motion and generalization of tissue properties.

1.3 Motivation. The presented SM research has hypothesized many mechanisms for the formation and distension of the syrinx cavity. However, the SM hypotheses lack pressure evidence required to develop a SM theory that is congruent with clinical observations and principles of mechanics. From a mechanical perspective, the clinical observation that mean syrinx pressure is equal or higher than the SAS pressure follows intuition since the syrinx fluid is contained within flexible SC tissue. If the pressure

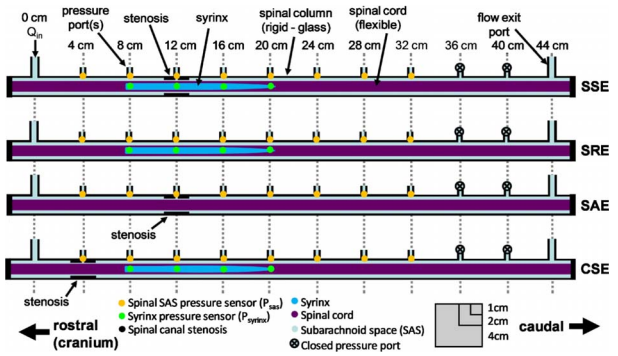

Fig. 1 Schematic diagram for each in vitro experiment indicating the location of the stenosis, syrinx, pressure sensors, spinal cord, flow input (Q_{in}), and flow exit port. (SSE=stenosis and syrinx experiment, SRE=stenosis removed experiment, SAE=stenosis alone experiment, and CSE=Chiari stenosis experiment.)

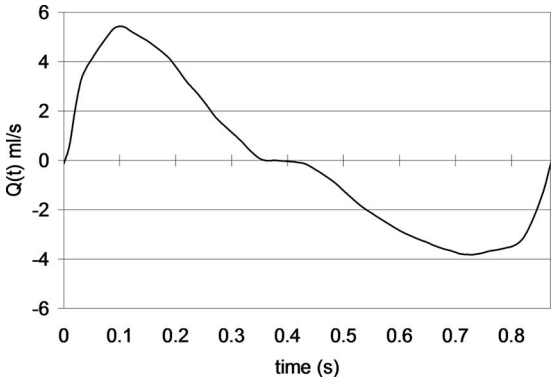

Fig. 2 The cyclic CSF flow waveform, $Q(t)$, input on the rostral end of each experiment by the computer controlled pulsatile pump

inside the syrinx was lower than the SAS, the syrinx would not expand in size but instead collapse. However, if fluid in the syrinx arises from the SAS, pressure in the SAS must be on average higher than the syrinx, at least locally, unless there is a one-way valve mechanism. Thus, the much pondered SM conundrum is posed. Many SM studies have stated that localized elevation in pulse and/or peak pressures can account for syrinx formation. However, a flexible SC would see these same increases also. Fluid will only move in the direction of lower pressure; thus, rise in pulse or peak pressure alone cannot account for bulk fluid movement into the syrinx, although it can account for movement of the cord.

The current hypotheses attribute SM pathophysiology to abnormal tissues and/or pressure environment. However, the pressure evidence to explain the pooling of fluid in the syrinx is lacking. Measurement of the pressure environment in an in vitro SM model was documented by Martin et al. [12]. However, this study lacked the hinging factor, a spinal stenosis. Herein, we present pressure measurements on a spinal stenosis SM flow model that closely represents the in vivo case to improve our understanding of the complex pressure environment associated with SM.

2 Methods

Four in vitro models were constructed; a schematic diagram of each of the models is shown in Fig. 1. The *stenosis and syrinx experiment (SSE)* was representative of a patient who has a moderate sized noncommunicating syrinx that distends both caudal and rostral to a spinal stenosis. This could be representative of a spinal CSF flow blockage that has resulted from vertebrae misalignment, tumor or arachnoid cyst development, or scarring of the spinal dura from various types of spinal trauma such as breakage of the vertebrae or bleeding. The *stenosis alone experiment (SAE)* was similar to SSE in that a spinal stenosis was present but different in that a spinal syrinx was not present. This is representative of a person who has suffered spinal trauma but has not developed a syrinx. The influence of stenosis location was examined in a *Chiari stenosis experiment (CSE)*, which had a stenosis located ~4 cm rostral to a noncommunicating syrinx, similar to the case when a CSF flow obstruction is present at the foramen magnum such as in a CM patient with SM. A *stenosis removal experiment (SRE)* was conducted in which the stenosis was removed while a noncommunicating syrinx remained, similar to that which may be present immediately after surgical removal of a spinal SAS flow blockage.

2.1 Diameters of SC, Syrinx, and SAS. A number of design criteria were identified from in vivo measurements on which to base the construction of the in vitro models. The spinal SAS geometry dimensions were based on MR measurements obtained from a patient with SM taken at 6 mm intervals along the spinal SAS previously reported by Martin et al. [12]. The MR images were processed using MIMICS (Materialise, Leuven, Belgium) software to create a 3D reconstruction of the syrinx and spinal SAS. The hydraulic diameters D_h of the syrinx, SC, and spinal SAS were computed with $D_h=4A_{cs}/P_{wet}$, where A_{cs} is the cross-sectional area and P_{wet} is the wetted perimeter of the region of interest. The average and standard deviations of the hydraulic diameters of the SAS, SC, and syrinx along the length of the spinal SAS were 15.6 ± 1.3 mm, 9.6 ± 1.3 mm, and 7.0 ± 1.1 mm, respectively. These values were rounded to the nearest millimeter and used for the diameters of the SAS, SC, and syrinx of the in vitro models. It has been observed that magnetic resonance imaging (MRI) of SM patients often indicates asymmetrical or multiple syringes [42,52,53]. Here, we chose to mimic a patient with a single noncommunicating syrinx that is nearly concentric with the SC of constant radius along its entire length.

2.2 Elastic Properties of the SC and Spinal SAS. For the construction of the SC, we assumed the tissue to be a homogeneous isotropic material, neglecting the material property variation between the gray and white matter and encasing meninges (dura and pia mater). Branching nerves from the SC were neglected in order to simplify construction and theoretical modeling of the system. The in vitro experiment SCs were constructed to have a Young's modulus of ~500 kPa, which is on the high side of published values. However, it can be noted that the experimentally measured mechanical properties of the SC vary widely when measured axially and transversally, the former likely being many orders of magnitude higher than the latter [54,55], and that measurements that remove the spinal dura likely underestimate the effective Young's modulus of the tissue [56]. Furthermore, the elastic modulus of biological tissues is largely strain rate dependent, and the time to test after excision increases the elastic modulus [57–59]. Thus, there is a wide variation in the measured values for SC mechanical properties, and the chosen modulus of 500 kPa was within the bounds of these measurements.

2.3 CSF Flow Waveform. The fluid used for the in vitro experiment was water due to the evidence that CSF is a Newtonian fluid, having viscosity about that of water [60]. The flow waveform $Q(t)$ for the experiments was similar to a realistic CSF flow waveform measured at the C2 level by MRI [18] (Fig. 2). Each CSF flow pulsation had approximately 1 ml of fluid with a maximum systolic and diastolic flow rate of 5.4 ml/s and 3.8 ml/s in the craniocaudal and caudocranial directions, respectively. This was computed from the syringe motion detected by a linear encoder at the flow pump input (Fig. 2).

2.4 Spinal Column Construction. The spinal column was

Table 1 Summary of experimental parameters. Tolerances are estimated based on manufacturing process tolerances and supplier specifications. (SSE=stenosis with syrinx experiment, CSE=Chiari stenosis experiment, SRE=stenosis removed experiment, and SAE=stenosis alone experiment.)

Variable	Dimension	Description
D_{SAS}	15.6 ± 0.3 mm	Diameter of subarachnoid space
D_{SC}	10.0 ± 0.2 mm	Diameter of spinal cord
T	1.2 ± 0.1 mm	Thickness of the glass tube used to form the spinal SAS
D_{syrinx}	7.0 ± 0.2 mm	Diameter of syrinx (constant until 28.7 mm from the caudal end of syrinx, tapered to 3.2 mm after that point)
L_{SC}	480 ± 2 mm	Length of spinal cord
L_{syrinx}	132 ± 1 mm	Length of syrinx
$L_{stenosis}$	20 ± 1 mm	Length of spinal stenosis (flow obstruction)
$ID_{stenosis}$	~ 10.7 mm	Approximate inner diameter of stenosis
$\%_{stenosis}$	$\sim 90\%$	Percent of spinal SAS blocked by stenosis
E_{SC}	SSE=315 kPa CSE=466 kPa SRE=830 kPa SAE=523 kPa	Young's modulus of spinal cord

formed by a glass tube with a 15.6 mm spinal SAS diameter (inner diameter (ID)), 1.2 mm thickness, and 48 cm length. Each model had ten pressure ports spaced at 4 cm intervals to measure the SAS pressure. A flow inlet port was used to connect the model to the computer controlled pulsatile pump, which simulated the desired CSF flow waveform. The CSF flow pulsation was baffled on the caudal end by a vertically oriented flow exit port (Fig. 1). The SCs for each experiment were centered and fixed on each end at $\sim 0\%$ tension using water tight end pins.

2.5 SC Construction. The SC for all four models was 480 mm long with a 10 mm diameter and was constructed using a flexible polymer (Sylgard 184, Dow Corning, Midland, MI), which was cast into a custom designed aluminum injection mold. A 7 mm diameter aluminum cylinder with slight tapering on the caudal end was positioned in the mold with a centering pin to form the syrinx cavity. The polymer used to make the SC had variable elastic properties based on the quantity of hardener used (20:1 mixture ratio). Because only one injection mold was constructed, each SC was cast separately, which resulted in slight variations in Young's modulus between each SC. Three cylindrical shaped straws were drawn from each casting batch and cured alongside each SC model. Static uniaxial stress-strain measurements were conducted on these straws to determine Young's modulus of each SC. A complete list of experimental parameters is provided in Table 1.

2.6 Bench-Top Experiment Description. The computer controlled an amplifier (model ASP-055-18, Copley Controls, Canton, MA) in an open voltage loop via Copley Controls CME2 software and was connected to the computer through an RS-232 cable (model ICUSB232, Radio Shack, Fort Worth, TX). The amplifier controlled the position of a linear motor (model TB1106, Copley Controls), which was connected to a 3 ml precision glass syringe (model 5340, Popper and Sons, New Hyde Park, NY). The syringe was filled with low viscosity spindle oil to reduce friction (Mobil velocite oil No. 6, Irving, TX). Oil from the syringe entered a custom designed oil-water boundary cylinder, and water exited the bottom of the cylinder due to having a lower density than the oil. The water traveled through a 7.6 m length, 6.35 mm ID rigid plastic tube (SPEB25 polyethylene, Watts, North Andover, MA) into the experiments through a network of y-type flow divisions (part 15-315-30B, Fischer Scientific, Pittsburgh, PA). A 20 mm length annular shaped stenosis was fashioned from rubber tubing (part 14-150-2F, 1/2 ID $\times$ 1/8 W $\times$ 3/4 in OD, Fischer Scientific) and was fitted into the rigid spinal column blocking $>90\%$ of the total SAS area when the system was at rest (when the syrinx was unpressurized and the pulsatile pump was stationary). A small hole was punched radially through the spinal stenosis leading out through an adjacent pressure port. The position of the stenosis is indicated for each experiment in Fig. 1. In addition, a 2 mm diameter syrinx catheter tube connected the syrinx to the outside environment, enabling catheter type pressure transducers (Millar Instruments SPR-524, 3.5F, 100 cm length, Houston, TX) to be guided inside the syrinx. During the experiments, the syrinx catheter tube was closed.

Catheter transducers (Millar Instruments SPR-524) measured SAS and syrinx pressure, $P(t)$, at distinct axial locations along each experiment. All pressure measurements are indicated relative to atmospheric pressure (gauge). The sensor voltage was amplified (model 880-0129, Millar Instruments) and then acquired via a data acquisition card (USB-6229, National Instruments), recorded in LABVIEW (Ver. 8.6, National Instruments), and processed using MATLAB (R2006b, Ver. 7.3, The MathWorks, Inc., Natick, MA). Data were taken at 10 kHz for a total of 10 s from all pressure sensors, while the pulsatile pump produced the CSF flow waveform, repeating every 870 ms (Fig. 2). Ensemble averaging of the pressure data from each sensor was performed for a total of ten CSF flow cycles using MATLAB.

Transmural pressure (TP) was obtained across the syrinx by subtraction of adjacent internal-external sensor signals in the syrinx and SAS ($TP(t)=P_{syrinx}(t)-P_{SAS}(t)$). LPD was calculated by subtracting the cervical from the lumbar SAS pressure at 4 cm and 32 cm, respectively ($LPD(t)=P_{SAS,32\ cm}(t)-P_{SAS,4\ cm}(t)$). Pulse pressure of a signal was obtained by subtracting the minimum from the maximum pressure during the CSF flow cycle. The pulse pressure of the TP gives an idea of the forces acting normal to the SC surface to expand or contract the syrinx cavity in the radial direction. LPD gives an idea of the longitudinal forces acting on the CSF system to suck or push CSF and/or tissue in the craniocaudal (negative LPD) or caudocranial direction (positive LPD).

3 Results

3.1 Temporal Pressure. Overall, the results indicated that the majority of pressure changes happen near the stenosis, and the magnitude of these changes are greater when a syrinx is present. The SAS pressure traces measured in SAE and SSE were noticeably different (Figs. 3 and 4). Traces are not shown in either of these plots beyond 20 cm because the pressure waveform observed in these regions resembled that at 20 cm. The pressure in the syrinx (12 cm) was similar to the adjacent SAS pressure (Fig. 4). Additionally, there was negligible axial pressure variation within the syrinx cavity for SSE, SRE, and CSE. This can be expected due to the fact that there was no flow obstruction inside

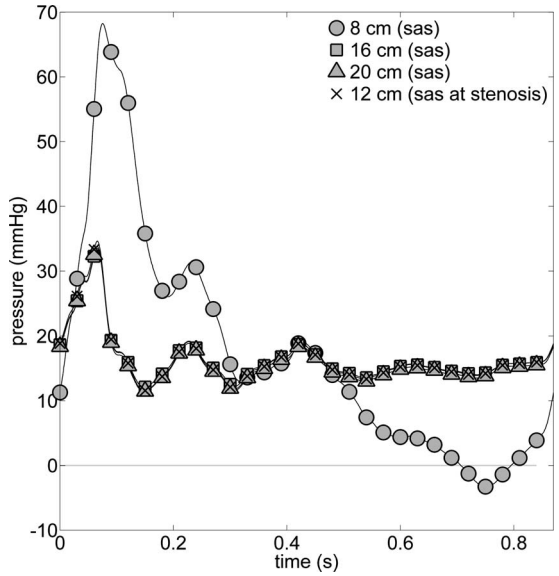

Fig. 3 SAS pressure changes over time measured at distinct axial locations in the stenosis alone experiment (SAE). Legend symbols identify pressure sensor location (sampling frequency was 10 kHz).

the syrinx cavity. Note that the pressure waveform change rostral to the stenosis at 4 cm and 8 cm in SAE and SSE did not change noticeably. Peak SAS pressure in SAE occurred earlier than in SSE by approximately 200 ms.

The cyclic maximum, average, and minimum pressures measured at different locations along the spinal SAS are given in Fig. 5. Note that the axis scale is different for each plot. In SSE, SRE, and CSE, pressure is also indicated in the syrinx. SAE indicates that both peak and average pressures decrease, moving craniocaudally rostral to the stenosis. Caudal to the stenosis, pressure remains nearly unchanged for SSE and SAE. Pulse pressures in SAE and SSE are much greater rostral to the stenosis than immediately caudal. Average pressure rostral to the stenosis in SSE was negative, while in SAE it remained positive. In contrast, during

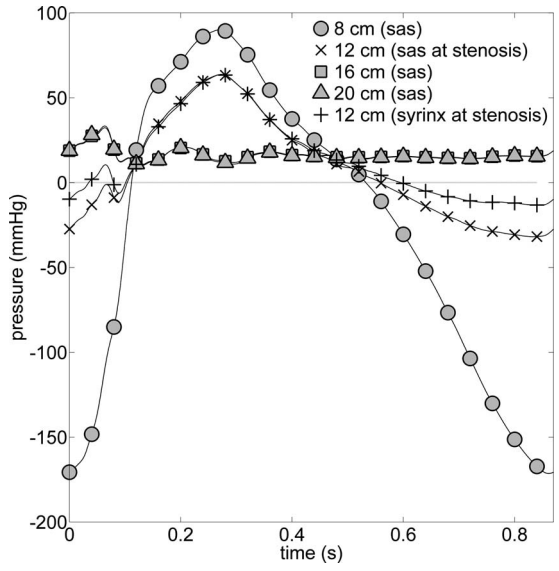

Fig. 4 Pressure changes over time measured at distinct axial locations in the SSE. Pressure in the syrinx at 12 cm is also indicated. Legend symbols identify pressure sensor location (sampling frequency was 10 kHz).

SRE and CSE, the maximum, average, and minimum pressures in the SAS and syrinx remained relatively uniform throughout the spinal SAS. Slightly larger pulse pressures were observed in CSE throughout the spinal SAS in comparison to SRE. Pressure was not obtained rostral to the stenosis in CSE experiment, but it is likely similar to that recorded rostral to the stenosis in SAE.

3.2 LPD. SSE had the greatest peak and pulse LPD during the CSF flow cycle (Fig. 6). A smaller, but substantial LPD was measured in SAE, while SRE had nearly zero LPD. LPD is not indicated for CSE in Fig. 6 because no pressure sensor was located rostral to the stenosis for CSE.

3.3 TP. The mean TP at the four adjacent sensor locations was positive rostral to the stenosis and negative caudal to the stenosis (Table 2). The magnitude of mean TP was significantly larger rostral to the stenosis. In addition, peak-to-peak values of TP were greatest rostral to and least at the stenosis. The TP at the two caudal measurement locations (16 cm and 20 cm) was nearly identical (Fig. 7). Additionally, the pressures rostral (4 cm) and caudal (16 cm and 20 cm) to the stenosis were out of phase. This can be observed when the TP is zero at times near 120 ms and 460 ms in Fig. 7. SRE and CSE demonstrated a much smaller TP fluctuation compared with SSE, having a maximum peak-to-peak variation of 2.1 mm Hg and 3.2 mm Hg, respectively (Table 2). Interestingly, in SRE, TP demonstrated the same out of phase phenomenon rostral and caudal to the stenosis as in SSE, while, in contrast, CSE was in phase. The pulse pressure in CSE increased craniocaudally but remained relatively uniform in SRE.

4 Discussion

This study quantified the temporal and spatial pressure distributions in flow experiments representative of four types of spinal stenosis conditions. These experiments were (1) a syrinx with stenosis at its midsection (SSE), (2) a syrinx with a proximal stenosis as exemplified by a CM (CSE), (3) a syrinx with stenosis removed (SRE), and (4) a stenosis alone without any syrinx (SAE). In our experiments, the presence and location of a spinal stenosis resulted in vastly different pressure conditions. Several aspects of the stenosed SAS were found to be worthy of inspection, including the influence of stenosis, a negligible Venturi effect, suck and slosh, bulk motion of the tissue and/or fluid, a diastolic valve mechanism, and SC tensioning.

Abnormal CSF pressure forces acting on the SC and/or brain caused by a SAS flow stenosis have been hypothesized to be an important factor contributing to syrinx formation and/or progression. This hypothesis is supported by the typical patient treatment, which involves removal of the stenosis by decompression surgery for patients with CM, spinal arachnoiditis, and other abnormalities in SAS geometry. Pain in a patient has also been postulated to be related to abnormal CSF pressure forces acting on the SC and hindbrain [2–4,6–8,61]. These forces govern the pressure gradients that result in the compression, tension, shearing, and/or movement of the SC tissue. Thus, discussion will focus on pressure gradients since in their absence, tissue is not expected to compress, move, or distend, as tissue is almost entirely composed of water and thus nearly incompressible.

4.1 Influence of Stenosis. The stenosis acted to increase and dissociate the CSF pressure in the SAS (Fig. 5). Similar pressure dissociation dynamics in the SAS were recorded by Williams in patients who had a CSF flow stenosis [5,23,62]. Pressure dissociation in the SAS was greatest in SSE and least in SRE. Maximum SC compression and distension occurred in SSE rostral to the stenosis and was much greater than with the CM type stenosis (CSE) or with the stenosis removed (SRE) (Fig. 5). However, in CSE, pulse pressures were greater throughout the entire system than when the stenosis was removed in SRE. In CSE, when the stenosis was rostral to the syrinx, the pressure fluctuation in the syrinx was nearly identical to that observed in the SAS, with a

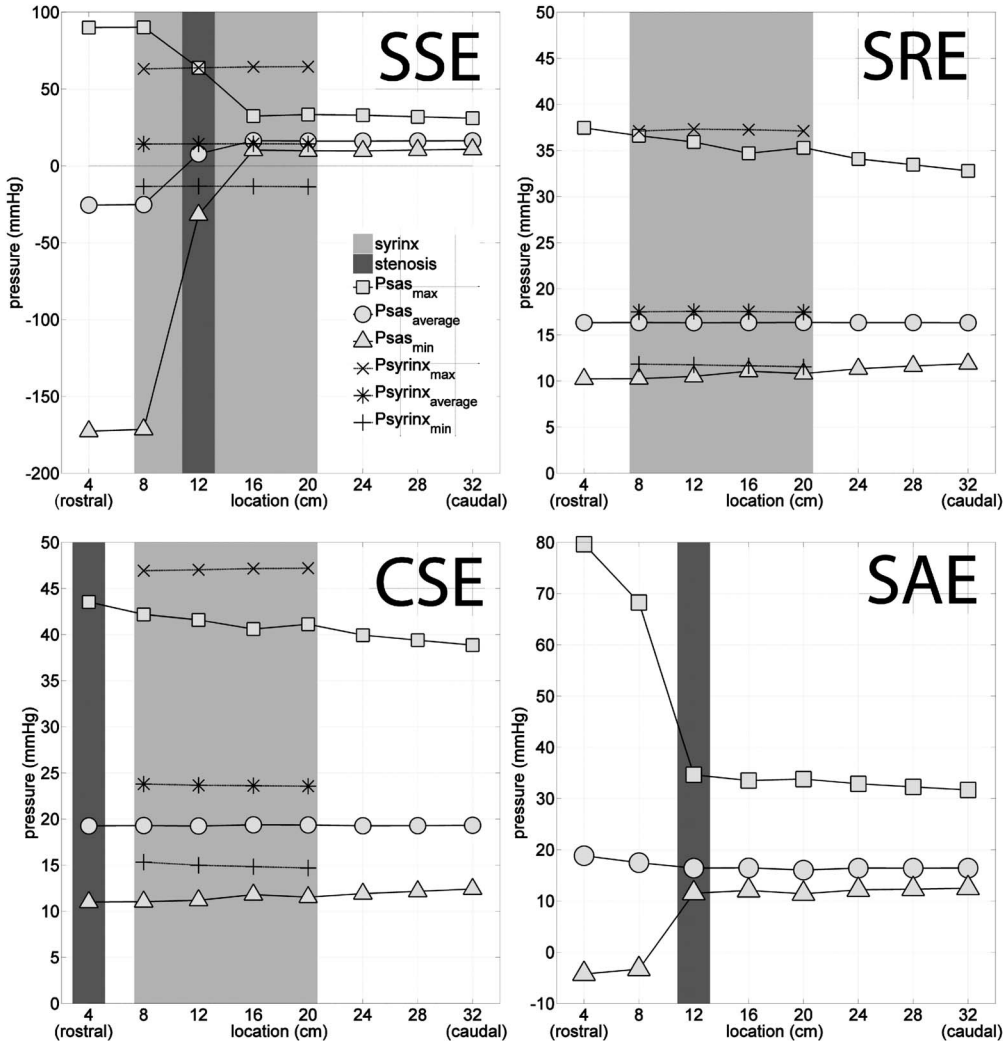

Fig. 5 Maximum, average, and minimum pressure in the SAS and syrinx (if present) for each experiment during the CSF pulsation (see SSE for legend). The light gray rectangle denotes location of the syrinx cavity (if present), and the dark gray vertical stripe denotes the location of the SAS stenosis. CSF flow was input at *x*-axis=0 cm location (skull base, rostral). Note, axis scale is different for each plot. (SSE=stenosis and syrinx experiment, SRE=stenosis removed experiment, SAE=stenosis alone experiment, and CSE=Chiari stenosis experiment).

potential mean offset based on syrinx pressurization.

The stenosis acted to significantly attenuate CSF pulsations originating from the pump (Figs. 3 and 5). Caudal to the stenosis, pressure fluctuations had little axial variation and relatively small attenuation (SSE, SAE, and CSE). Bilston et al. produced a numerical model having similar pressure pulse attenuation by using a purely resistive approach, with the stenosis acting as a porous plug [51]. Levine also hypothesized a similar CSF pressure drop across a SAS flow blockage [44]. Bilston et al. hypothesized that elevations in SAS pressure due to arachnoiditis "may facilitate flow into the SC and enhance syrinx formation" [51]. Note that elevation in pressure on its own would not support movement of fluid or tissue, as spatial gradients in pressure are required. The transient low pressure rostral to the stenosis in SSE, CSE, and SAE (Figs. 3–5) supports work by Oldfield et al., in which a low pressure zone in the lower hindbrain during diastole causes a ball-valve effect at the lower aspect of the cerebellar tonsils, pulling them caudally and thereby obstructing CSF flow through the region [31].

4.2 Negligible Venturi Effect. The stenosis did not cause a substantial level of Venturi effect in any of the in vitro experiments. Less severe stenoses should be examined to determine the importance, if any, of the Venturi effect, a mechanism proposed to help explain SM pathogenesis [32]. In SAE, when a syrinx was not present, the mean SAS pressure dropped at the stenosis site and did not recover (Figs. 3 and 5), as would be the case if a Venturi effect was significant. The greatest level of instantaneous pressure recovery after the stenosis (0.59 mm Hg) was only 1.3% of the maximum pressure drop preceding the stenosis (44.4 mm Hg), where the percentage was calculated by dividing pressure change caudal to the stenosis by the maximum pressure change rostral to the stenosis $(100[P_{\mathrm{SAS,16\ cm}}(t) - P_{\mathrm{SAS,12\ cm}}(t)]/\max[P_{\mathrm{SAS,8\ cm}}(t) - P_{\mathrm{SAS,12\ cm}}(t)])$. Interestingly, when a syrinx was present in the SC (SSE), the mean pressure in the SAS at the stenosis site increased (Figs. 4 and 5), opposite to what would be expected by the Venturi effect. Similar to SAE, the pressure recovery caudal to the stenosis was negligible throughout the CSF flow cycle. As such, the presence of a spinal stenosis and syrinx can produce an unexpected pressure environment. Thus, the stenosis did not cause a significant Venturi effect but instead

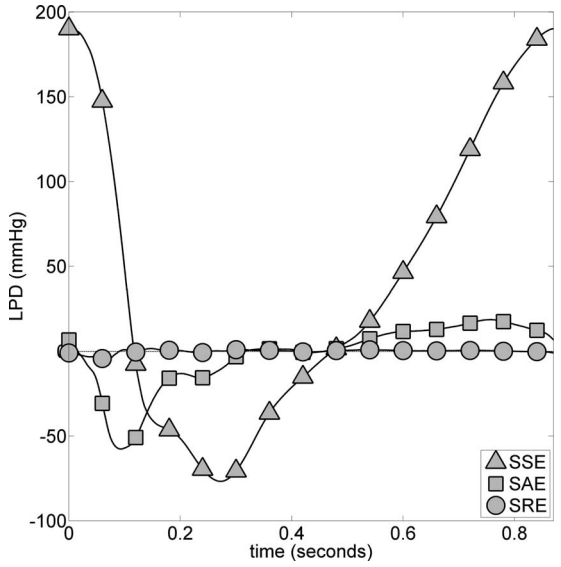

Fig. 6 Longitudinal pressure dissociation (LPD) (lumbar-cervical) measured in the SAS during the CSF flow pulsation ($LPD(t) = P_{SAS,4\ cm}(t) - P_{SAS,32\ cm}(t)$). Sampling frequency for each experiment was 10 kHz. (SSE=stenosis and syrinx experiment, SAE=stenosis alone experiment, and SRE=stenosis removed experiment.)

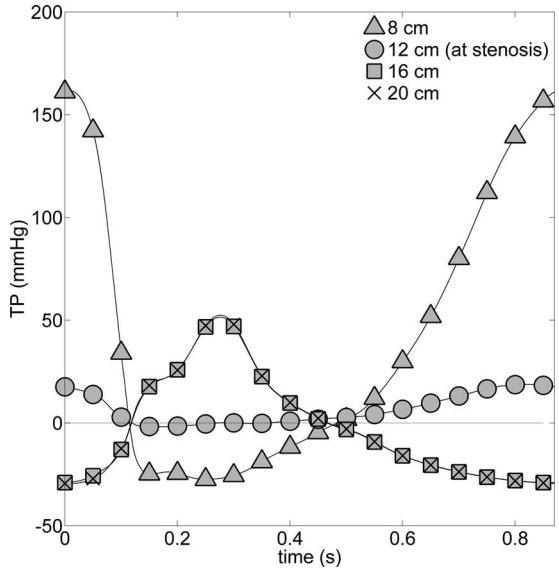

Fig. 7 TP in the SSE measured at four adjacent sensor locations along the syrinx during the CSF flow pulsation ($TP(t) = P_{syrinx}(t) - P_{SAS}(t)$). Positive pressure trace indicates that the pressure in the syrinx is greater than the SAS at adjacent measurement locations. Negative pressure trace indicates that syrinx pressure is less than the SAS. Legend symbols identify pressure sensor location (sampling frequency was 10 kHz).

acted as a CSF pressure pulse attenuator. The unsteady flow and viscous losses in the coaxial elastic tube system are likely responsible.

4.3 Pressure in the Syrinx. The unsteady pressure distribution within the syrinx had little axial variation in all of the experiments, while unsteady pressure in the SAS varied widely (Figs. 5 and 6). The differences between the syrinx and SAS pressure distribution resulted in significant TPs (Fig. 7). Since SSE had the largest LPD in the SAS (Fig. 6), it also had the largest TP. The pressure trace in the syrinx closely followed the nearby SAS pressure for CSE and SRE (Fig. 5). Syrinx pressure in SSE most closely followed the SAS pressure at the stenosis location (Fig. 4), seemingly independent of the large pressure fluctuations immediately rostral to the stenosis and yet adjacent to the syrinx.

4.4 Suck and Slosh. The axial distribution of TP was found to vary in direction and magnitude along the syrinx cavity and with the presence and location of a stenosis (Fig. 7). In SSE, the stenosis caused the syrinx to be compressed on one side while expanded on the other. This effect was greatest during diastole (caudocranial CSF flow in SAS) and was also true in the mean for SSE (Table 2 and Fig. 7). A significant level of LPD was present in SSE and SAE, while in SRE LPD was nearly zero (Fig. 6). These findings support the suck and slosh mechanisms postulated by Williams, which attributed syrinx formation and expansion to LPD caused by CSF flow obstruction [5]. Note that in the case when the stenosis was located entirely rostral to the syrinx (CSE), analogous to CM, little LPD and TP were measured along the syrinx cavity. However, in Williams' work, significant LPD was observed in CM patients. This discrepancy may be due to the experiment's inability to reproduce any piston type action of the cerebellar tonsils at the craniocervical junction. Thus, the CSE findings imply that if large TPs exist in CM patients with syrinxes, they likely cannot be attributed to a stationary flow blockage at the craniospinal junction alone. Rather, a valve action near the syrinx cavity would be required to produce large TPs.

4.5 Bulk CSF Movement. Mean nonzero TP will result in syrinx size change (positive=reduction, negative=growth). This is assuming that tissue properties are such that resistance to transmural flow (permeability) is uniform along the syrinx cavity. Significant TP was quantified, which could drive bulk fluid into the syrinx cavity in SSE (see negative mean TP values in Table 2). In the case of CSE and SRE, the TPs were smaller and consistently positive and thus would not support bulk fluid movement into the syrinx (see Table 2 and Fig. 7). However, in SSE fluid could be sucked into the syrinx on the caudal end and retained on the rostral end if the cord permeability was greater caudal to the stenosis. Given the difference in biomechanical stresses experienced by the SC on opposite ends of the stenosis, one could hypothesize that tissue properties, such as permeability and compliance, may also be different. However, the mean outward directed TP was significantly greater than inward direct TP over the entire syrinx cavity (Table 2). Thus, the fluid dynamics would suggest syrinx emptying unless a large variation in SC permeability or a

Table 2 Mean and pulse (maximum-minimum) of TP measurements

	Transmural pressure in mm Hg ($P_{syrinx} - P_{SAS}$)									
	4 cm		8 cm		12 cm		16 cm		Average	
Experiment	Mean	Pulse	Mean	Pulse	Mean	Pulse	Mean	Pulse	Mean	Pulse
SSE	39.4	189.2	6.4	20.7	−2.0	80.7	−1.9	82.0	10.5	93.1
CSE	4.5	1.0	4.4	1.9	4.2	3.6	4.2	3.2	4.3	2.4
SRE	1.2	1.7	1.2	1.0	1.2	2.1	1.1	1.4	1.2	1.5

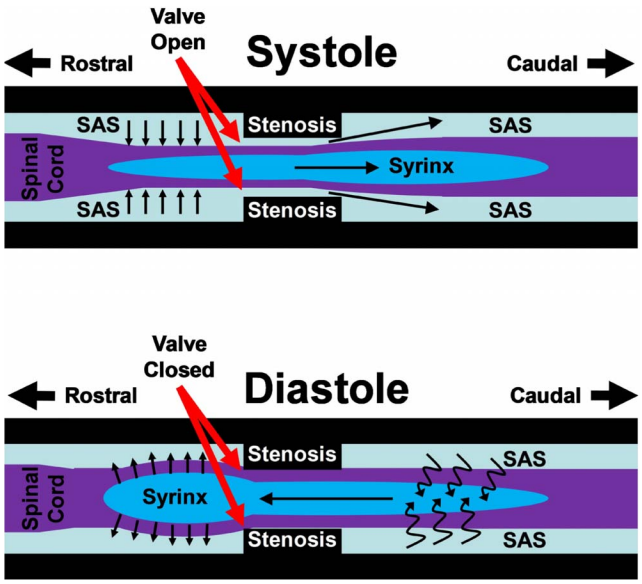

Fig. 8 Illustration of the diastolic valve mechanism produced by the interaction of the syrinx and stenosis during the CSF pulsation in systole (top-valve open) and diastole (bottom-valve closed) in SSE. Note that valve closure during diastole was not continuous. CSF must return to the rostral end of the SAS to satisfy conservation of mass.

one-way valve was present. Axial variation in SC tissue permeability was supported in a study by Brodbelt et al., who measured greater CSF tracer movement into the cord at the level of the syrinx (C8) than rostral to it (C5) [33]. It would be useful to conduct a detailed histological study of axial variation in tissue permeability of the SC and/or syrinx wall.

4.6 Diastolic Valve Mechanism (SSE Only). The SSE results indicated that the interaction of a stenosis and syrinx caused a diastolic valve mechanism (Fig. 8) that was characterized by a greater resistance to caudocranial CSF flow in the SAS during diastole than during systole (craniocaudal). Images from a video of the syrinx ballooning and contraction in SSE during the cardiac cycle are shown in Fig. 9. The motion of the syrinx wall was asymmetric and estimated visually to be a maximum of ~1 mm and 3 mm caudal and rostral to the stenosis, respectively. The magnitude of this motion is similar to that observed in vivo by Heiss et al. (~0.6 mm intra-operative) [1] and Lichtor et al. (~1.2 mm pre-operative) [63]. Asymmetric syrinx motion of ~150 μm was reported by Martin et al. in an in vitro experiment without a spinal stenosis [12]. In systole, the syrinx was compressed (Figs. 8 and 9), which reduced resistance to caudal CSF movement in the SAS through the SAS stenosis region. Systolic compression of the rostral end of the syrinx was also observed in vivo by Heiss et al. [1] and detailed by Oldfield et al. [31]. At the onset of diastole, the SC was pulled outward (Fig. 9) by large positive TP rostral to the stenosis (Fig. 7 and Table 2), which resulted in greater resistance to CSF flow in the SAS returning to the cranium. The net influence was to depress the average SAS pressure rostral to the stenosis (Fig. 5, SSE). Fluid was then sucked caudocranially through the syrinx, ballooning the rostral end. Note that valve closure during diastole was not continuous (Fig. 8). CSF must return to the rostral end of the SAS to satisfy the conservation of mass. Caudocranial suction of fluid in the syrinx resulted in a negative TP caudal to the stenosis (Fig. 7 and Table 2), which would provide a pressure gradient to direct bulk flow into the syrinx cavity on the caudal end. Thus, the syrinx, in conjunction with a stenosis, was shown to act with a diastolic valve mechanism.

The global influence of the diastolic valve mechanism was to cause a sustained low TP zone in the syrinx caudal to the stenosis, which was counterbalanced by a zone of greater positive TP rostral to the stenosis (Table 2). Thus, the diastolic valve mechanism results support syrinx size reduction. However, this mechanism is likely sensitive to tissue properties, size, and relative placement of the syrinx and stenosis as well as the CSF flow waveform. Under certain conditions, it is possible that average negative TPs could occur, which would support fluid accumulation in the syrinx. The negative TPs observed could work in conjunction with a one-way valve encouraging extracellular fluid movement into the syrinx, such as the arterial pumping mechanism proposed by Bilston et al.

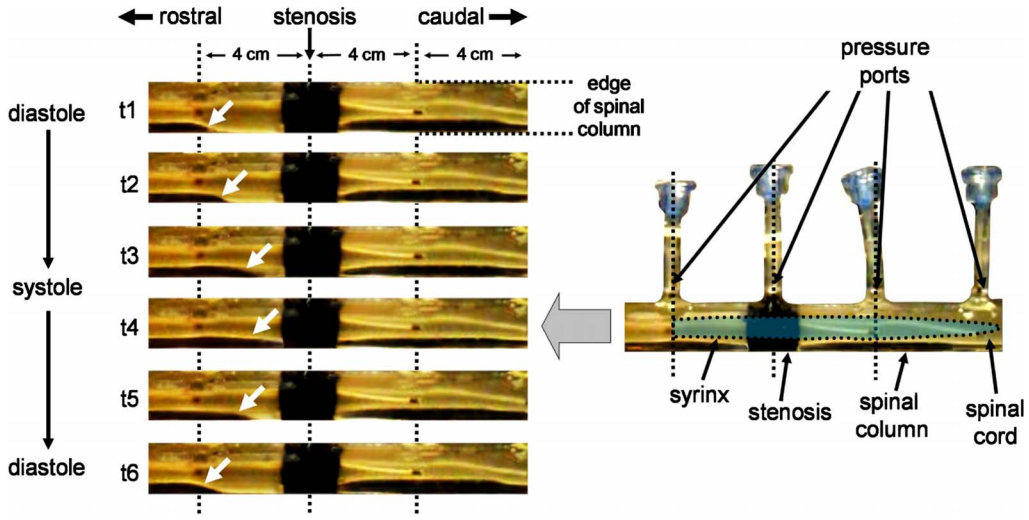

Fig. 9 Images from a video of the SSE at different time points (t1–t6) during the CSF flow pulsation (left). Approximate locations of the syrinx, stenosis, pressure ports, and spinal cord are indicated in the diagram (right). Regions with the greatest spinal cord movement are indicated by white arrows in each video frame. Note that the spinal cord motion is asymmetric, flexing more on the bottom side than on the top. Also, greater spinal cord motion is present rostral to the stenosis than caudal. The outward ballooning of the syrinx is best observed during diastole at t1 and t6 in the region 4 cm rostral to the stenosis. Syrinx contraction can be observed during systole from t3 to t5 (complete video is provided at www.csflab.com/video/20080610_SSE_model.AVI).

[17,43]. The diastolic valve mechanism also demonstrates some of the ideas brought forth by Grietz [32] and Grietz et al. [64], such as the "milking effect." One important aspect of the results observed in SSE is that the mechanism was not symmetric across the stenosis but rather preferential to caudocranial flow in the syrinx and craniocaudal flow in the SAS.

The diastolic valve mechanism's ability to cause significant LPD, elevated TP, and a sustained low pressure zone rostral to the stenosis may have a number of important influences on the craniospinal system. This mechanism may help to provide an underlying reason for tissue changes such as myelopathy, edema, gliosis, vascular wall thickening, and/or ischemia, which have been identified by a number of researchers [11,44,65] and by some termed presyringomyelia [66]. In one study, Klekamp et al. noted an "interstitial type of edema in the central gray matter below the area of scarring in the cat cervical cord" and attributed it to the abnormal CSF and extracellular fluid flow dynamics [11]. Milhorat et al. [67] and Milhorat [68] also noted that extra canicular syrinxes are lined with gliosis and are different from canicular syringes, which are lined with complete or discontinuous ependymal lining, and that this suggests a different etiology [33]. While the diastolic valve mechanism was only present in SSE, similar pressure gradients may occur between the minute extracellular spaces in the SC parenchyma and the SAS when a spinal stenosis is present. However, in order for the diastolic valve mechanism to function, the SC would still be required to be compressed, however minutely, during systole and expanded during diastole at the stenosis location. Thus, the mechanical properties of the cord and canal could play an important role, limiting the extent to which any such valve mechanism could function.

The extent of influence that the diastolic valve mechanism has on the craniospinal system is unclear but could be far reaching. It is likely that alterations in LPD, TP, and depression in average SAS pressure rostral to the stenosis will not change the mean arterial blood pressure in the cranium, but ICP may be influenced. Communication between the CSF pressure alterations caused by the diastolic valve effect and the venous system could also be important. These changes may result in the alteration of cerebrovascular resistance, cerebral perfusion pressure, and cerebral blood flow and may influence craniospinal compliance.

4.7 Spinal Cord Tensioning (Tight Filum Terminale, SSE Only). A secondary effect of the diastolic valve mechanism was to caudocranially tension the SC. This was the result of the net positive LPD (Fig. 6, SSE) and the TP rostral to the stenosis causing the syrinx to balloon outward (Figs. 7–9). The caudocranial tensioning of the SC could be physically observed by turning the CSF flow pump off. When the pump was turned off, the SC shifted craniocaudally to a more relaxed state. Caudocranial tensioning of the SC due to the diastolic valve mechanism is particularly interesting given the controversy surrounding the relationship, if any, between tethered cord, SM, CM, and scoliosis [69].

4.8 Comparison of In Vitro and In Vivo Measurements. The pressure measurements can be compared with in vivo in terms of temporal pressure maximum, minimum, TP, and LPD. The pressure measurements in the experiments varied widely with maximum and minimum values of 80 mm Hg and −170 mm Hg, respectively (see Fig. 5, negative values are below atmospheric pressure). While these pressures may be exaggerated due to the simplification of the experimental configuration, large peak and pulse pressures in vivo have been reported in the literature [1,3,4,6,7,9]. Sansur et al. found the maximum peak pressure in the SAS in response to jugular compression to be ~40 mm Hg and during coughing to be ~125 mm Hg [70]. Williams measured the pressure in the SAS during coughing to be ~80 mm Hg [5]. TP in a patient during coughing was recorded by Williams between the syrinx and SAS of nearly 40 mm Hg [5]. Hall et al. measured mean pressure inside the syrinx to be 7 mm Hg, while the SAS CSF pulsation was only 0.5–1 mm Hg [9,44], and Milhorat et al. recorded subatmospheric syrinx pressure after drainage [6].

LPD was measured in vivo by Williams on 37 SM patients with hindbrain abnormality. Williams found that 24 of these patients had a "valvular action…allowing fluid to move upwards easily but only with more difficulty and delay…move downward again" [5]. The characteristic valvular action was manifest in LPD being transmitted quickly up the spinal SAS during the initial cough phase (<1 s) but slowly afterward (>10 s). The maximum LPD during coughing onset was measured to be ~100 mm Hg ($P_{\text{lumbar}}-P_{\text{cervical}}$). LPD can also be obtained from the intraoperative jugular compression tests reported by Heiss et al., for patients with SM and CM (Queckenstedt's test), to be as large as −20 mm Hg ($P_{\text{lumbar}}-P_{\text{ICP}}$) [1]. The opposite sign of LPD in Heiss' results in comparison to Williams' is because Queckenstedt's test has the opposite direction of pressure influence on the spinal SAS as coughing [5].

In SSE and SAE, large fluctuations in LPD were recorded during the CSF flow cycle (Fig. 6). While the LPD fluctuations in SSE and SAE were large, they were near the bounds of LPD measurements recorded in vivo during coughing and valsalva. It is likely that the large positive LPD recorded in SSE was due to CSF flow being volume rather than pressure controlled. The measurements may also be exaggerated in comparison to in vivo due to the use of a rigid glass tube for the spinal SAS, the large extent of CSF flow obstruction at the stenosis (~90%), and the experiment's lack of branching nerves and vessels.

The cited literature suggests that the in vivo spinal SAS pressure environment can vary widely, making it difficult to pick a best case for comparison. While the pressure magnitude may not be the same as in vivo, the global dynamics and trends are expected to be representative of those present in the craniospinal system with flow blockage and/or syrinx. The detailed in vitro pressure measurements are useful because they cannot be acquired in vivo given the invasive nature necessary to obtain them. Additionally, computational fluid-structure interaction models [13–19,48,49,51] are continually improving, and the measurements described herein provide data for comparison.

4.9 Experimental Limitations. Care was taken to perform the experiments as close to in vivo conditions as possible. However, simplifications were required. The dura, pia, white, and gray matter of the SC were lumped into one uniform body, neglecting branching nerves and perfusing vessels. The spinal SAS was assumed to be nearly rigid, being composed of glass. Dimensions of the SC and SAS were simplified to be circular and concentric. The syrinx was located concentrically within the SC, and the stenosis blocked ~90% of the SAS around the SC (see Table 1 for dimensions). Additionally, the CSF flow waveform (Fig. 2) was based on in vivo flow measurements obtained at the C2 level on a patient with SM and was volume controlled rather than pressure controlled. Overall, the in vitro experiments were simplified with respect to geometry, flow input, and material properties. Even under such assumptions, these experiments provide insight to the complex pressure environment present in the spinal SAS with a stenosis and/or syrinx present.

5 Conclusions

The in vitro pressure data and analyses provide valuable information about cerebrospinal fluid hydrodynamics and demonstrate the complexity of the fluid-structure interaction present in the spinal SAS with a stenosis and syrinx. The presence and location of the stenosis and syrinx were found to have critical impact on the pressure environment. The interaction of the syrinx and stenosis resulted in a diastolic valve mechanism and rostral tensioning of the SC. In all experiments, the stenosis was shown to increase and dissociate SAS pressure, while longitudinal pressure in the syrinx remained nearly constant. These pressure measurements highlight

the importance of the mechanical properties of the SC and spinal SAS, including compliance and tissue permeability. In addition, these results provide data for comparison with computational models of the spinal SAS. Further research examining the influence of stenosis size and location in more sophisticated in vitro models, as well as better understanding of craniospinal tissue properties, is warranted.

Acknowledgment

This work was supported by the American Syringomyelia Alliance Project. The authors thank Dr. Chris Bertram (University of New South Whales) for his detailed and insightful review of the manuscript and Dr. John Heiss (Surgical Neurology Branch, NINDS) for his discussion.

References

[1] Heiss, J. D., Patronas, N., DeVroom, H. L., Shawker, T., Ennis, R., Kammerer, W., Eidsath, A., Talbot, T., Morris, J., Eskioglu, E., and Oldfield, E. H., 1999, "Elucidating the Pathophysiology of Syringomyelia," J. Neurosurg., **91**(4), pp. 553–562.
[2] Williams, B., 1976, "Cerebrospinal Fluid Pressure Changes in Response to Coughing," Brain, **99**(2), pp. 331–346.
[3] Williams, B., 1981, "Simultaneous Cerebral and Spinal Fluid Pressure Recordings. 2. Cerebrospinal Dissociation With Lesions at the Foramen Magnum," Acta Neurochir., **59**(1–2), pp. 123–142.
[4] Williams, B., 1981, "Simultaneous Cerebral and Spinal Fluid Pressure Recordings. I. Technique, Physiology, and Normal Results," Acta Neurochir., **58**(3–4), pp. 167–185.
[5] Williams, B., 1980, "On the Pathogenesis of Syringomyelia: A Review," J. R. Soc. Med., **73**(11), pp. 798–806.
[6] Milhorat, T. H., Capocelli, A. L., Jr., Kotzen, R. M., Bolognese, P., Heger, I. M., and Cottrell, J. E., 1997, "Intramedullary Pressure in Syringomyelia: Clinical and Pathophysiological Correlates of Syrinx Distension," Neurosurgery, **41**(5), pp. 1102–1110.
[7] Williams, B., 1980, "Experimental Communicating Syringomyelia in Dogs After Cisternal Kaolin Injection. Part 2. Pressure Studies," J. Neurol. Sci., **48**(1), pp. 109–122.
[8] Williams, B., and Bentley, J., 1980, "Experimental Communicating Syringomyelia in Dogs After Cisternal Kaolin Injection. Part 1. Morphology," J. Neurol. Sci., **48**(1), pp. 93–107.
[9] Hall, P., Turner, M., Aichinger, S., Bendick, P., and Campbell, R., 1980, "Experimental Syringomyelia: The Relationship Between Intraventricular and Intrasyrinx Pressures," J. Neurosurg., **52**(6), pp. 812–817.
[10] Stoodley, M. A., Brown, S. A., Brown, C. J., and Jones, N. R., 1997, "Arterial Pulsation-Dependent Perivascular Cerebrospinal Fluid Flow Into the Central Canal in the Sheep Spinal Cord," J. Neurosurg., **86**(4), pp. 686–693.
[11] Klekamp, J., Volkel, K., Bartels, C. J., and Samii, M., 2001, "Disturbances of Cerebrospinal Fluid Flow Attributable to Arachnoid Scarring Cause Interstitial Edema of the Cat Spinal Cord," Neurosurgery, **48**(1), pp. 174–185.
[12] Martin, B. A., Kalata, W., Loth, F., Royston, T. J., and Oshinski, J. N., 2005, "Syringomyelia Hydrodynamics: An In Vitro Study Based on In Vivo Measurements," J. Biomech. Eng., **127**(7), pp. 1110–1120.
[13] Carpenter, P. W., Berkouk, K., and Lucey, A. D., 2003, "Pressure Wave Propagation in Fluid-Filled Co-Axial Elastic Tubes. Part 2: Mechanisms for the Pathogenesis of Syringomyelia," ASME J. Biomech. Eng., **125**(6), pp. 857–863.
[14] Berkouk, K., Carpenter, P. W., and Lucey, A. D., 2003, "Pressure Wave Propagation in Fluid-Filled Co-Axial Elastic Tubes. Part 1: Basic Theory," ASME J. Biomech. Eng., **125**(6), pp. 852–856.
[15] Bertram, C. D., Bilston, L. E., and Stoodley, M. A., 2008, "Tensile Radial Stress in the Spinal Cord Related to Arachnoiditis or Tethering: A Numerical Model," Med. Biol. Eng. Comput., **46**(7), pp. 701–707.
[16] Bertram, C. D., Brodbelt, A. R., and Stoodley, M. A., 2005, "The Origins of Syringomyelia: Numerical Models of Fluid/Structure Interactions in the Spinal Cord," ASME J. Biomech. Eng., **127**(7), pp. 1099–1109.
[17] Bilston, L. E., Fletcher, D. F., Brodbelt, A. R., and Stoodley, M. A., 2003, "Arterial Pulsation-Driven Cerebrospinal Fluid Flow in the Perivascular Space: A Computational Model," Comput. Methods Biomech. Biomed. Eng., **6**(4), pp. 235–241.
[18] Loth, F., Yardimci, M. A., and Alperin, N., 2001, "Hydrodynamic Modeling of Cerebrospinal Fluid Motion Within the Spinal Cavity," ASME J. Biomech. Eng., **123**(1), pp. 71–79.
[19] Chang, H. S., and Nakagawa, H., 2003, "Hypothesis on the Pathophysiology of Syringomyelia Based on Simulation of Cerebrospinal Fluid Dynamics," J. Neurol., Neurosurg. Psychiatry, **74**(3), pp. 344–347.
[20] Alperin, N. J., Lee, S. H., Loth, F., Raksin, P. B., and Lichtor, T., 2000, "MR-Intracranial Pressure (ICP): A Method to Measure Intracranial Elastance and Pressure Noninvasively by Means of MR Imaging: Baboon and Human Study," Radiology, **217**(3), pp. 877–885.
[21] Gardner, W. J., and Angel, J., 1958, "The Mechanism of Syringomyelia and Its Surgical Correction," Clin. Neurosurg., **6**, pp. 131–140.
[22] Gardner, W. J., 1965, "Hydrodynamic Mechanism of Syringomyelia: Its Relationship to Myelocele," J. Neurol. Neurosurg. Psychiatry, **28**, pp. 247–259.
[23] Williams, B., 1969, "The Distending Force in the Production of Communicating Syringomyelia," Lancet, **294**(7622), pp. 696–697.
[24] Williams, B., 1978, "A Critical Appraisal of Posterior Fossa Surgery for Communicating Syringomyelia," Brain, **101**(2), pp. 223–250.
[25] Itabashi, T., 1990, "Quantitative Analysis of Cervical CSF and Syrinx Fluid Pulsations," Nippon Seikeigeka Gakkai Zasshi, **64**(7), pp. 523–533.
[26] Enzmann, D. R., O'Donohue, J., Rubin, J. B., Shuer, L., Cogen, P., and Silverberg, G., 1987, "CSF Pulsations Within Nonneoplastic Spinal Cord Cysts," AJR, Am. J. Roentgenol., **149**(1), pp. 149–157.
[27] Ball, M. J., and Dayan, A. D., 1972, "Pathogenesis of Syringomyelia," Lancet, **300**(7781), pp. 799–801.
[28] Weller, R. O., 1998, "Pathology of Cerebrospinal Fluid and Interstitial Fluid of the CNS: Significance for Alzheimer Disease, Prion Disorders and Multiple Sclerosis," J. Neuropathol. Exp. Neurol., **57**(10), pp. 885–894.
[29] Zhang, E. T., Inman, C. B., and Weller, R. O., 1990, "Interrelationships of the Pia Mater and the Perivascular (Virchow-Robin) Spaces in the Human Cerebrum," J. Anat., **170**, pp. 111–123.
[30] Stoodley, M. A., Jones, N. R., and Brown, C. J., 1996, "Evidence for Rapid Fluid Flow From the Subarachnoid Space Into the Spinal Cord Central Canal in the Rat," Brain Res., **707**(2), pp. 155–164.
[31] Oldfield, E. H., Muraszko, K., Shawker, T. H., and Patronas, N. J., 1994, "Pathophysiology of Syringomyelia Associated With Chiari I Malformation of the Cerebellar Tonsils. Implications for Diagnosis and Treatment," J. Neurosurg., **80**(1), pp. 3–15.
[32] Greitz, D., 2006, "Unraveling the Riddle of Syringomyelia," Neurosurg. Rev., **29**(4), pp. 251–264.
[33] Brodbelt, A. R., Stoodley, M. A., Watling, A. M., Tu, J., and Jones, N. R., 2003, "Fluid Flow in an Animal Model of Post-Traumatic Syringomyelia," Eur. Spine J., **12**(3), pp. 300–306.
[34] Stoodley, M. A., 2000, "Pathophysiology of Syringomyelia," J. Neurosurg., **92**(6), pp. 1069–1070.
[35] Brodbelt, A. R., Brown, C. J., and Jones, N. R., 2001, "Time and Dose Profiles of Experimental Excitotoxic Post-Traumatic Syringomyelia (Abstract)," Aust. N. Z. J. Surg., **71**(A66).
[36] Brodbelt, A. R., Stoodley, M. A., Watling, A. M., Tu, J., Burke, S., and Jones, N. R., 2003, "Altered Subarachnoid Space Compliance and Fluid Flow in an Animal Model of Posttraumatic Syringomyelia," Spine, **28**(20), pp. E413–E419.
[37] Stoodley, M. A., Gutschmidt, B., and Jones, N. R., 1999, "Cerebrospinal Fluid Flow in an Animal Model of Noncommunicating Syringomyelia," Neurosurgery, **44**(5), pp. 1065–1075.
[38] Stoodley, M. A., Jones, N. R., Yang, L., and Brown, C. J., 2000, "Mechanisms Underlying the Formation and Enlargement of Noncommunicating Syringomyelia: Experimental Studies," Neurosurg. Focus, **8**(3), pp. 1–7.
[39] Storer, K. P., Toh, J., Stoodley, M. A., and Jones, N. R., 1998, "The Central Canal of the Human Spinal Cord: A Computerised 3-D Study," J. Anat., **192**(4), pp. 565–572.
[40] Brodbelt, A. R., and Stoodley, M. A., 2003, "Post-Traumatic Syringomyelia: A Review," J. Clin. Neurosci., **10**(4), pp. 401–408.
[41] Wagner, F. C., Jr., and Stewart, W. B., 1981, "Effect of Trauma Dose on Spinal Cord Edema," J. Neurosurg., **54**(6), pp. 802–806.
[42] Davis, C. H., and Symon, L., 1989, "Mechanisms and Treatment in Post-Traumatic Syringomyelia," Br. J. Neurosurg., **3**(6), pp. 669–674.
[43] Bilston, L. E., Stoodley, M. A., and Fletcher, D. F., 2009, "The Influence of the Relative Timing of Arterial and Subarachnoid Space Pulse Waves on Spinal Perivascular Cerebrospinal Fluid Flow as a Possible Factor in Syrinx Development," J. Neurosurg., **112**, pp. 808–813.
[44] Levine, D. N., 2004, "The Pathogenesis of Syringomyelia Associated With Lesions at the Foramen Magnum: A Critical Review of Existing Theories and Proposal of a New Hypothesis," J. Neurol. Sci., **220**(1–2), pp. 3–21.
[45] Klekamp, J., 2002, "The Pathophysiology of Syringomyelia–Historical Overview and Current Concept," Acta Neurochir., **144**(7), pp. 649–664.
[46] Perrin, R. G., and Fehlings, M., 2004, "The Etiology of Syringomyelia in Association With Lesions of the Foramen Magnum," J. Neurol. Sci., **220**(1–2), pp. 1–2.
[47] Iskandar, B. J., Hedlund, G. L., Grabb, P. A., and Oakes, W. J., 1998, "The Resolution of Syringohydromyelia Without Hindbrain Herniation After Posterior Fossa Decompression," J. Neurosurg., **89**(2), pp. 212–216.
[48] Cirovic, S., 2009, "A Coaxial Tube Model of the Cerebrospinal Fluid Pulse Propagation in the Spinal Column," ASME J. Biomech. Eng., **131**(2), p. 021008.
[49] Cirovic, S., Walsh, C., and Fraser, W. D., 2002, "Wave Propagation in a System of Coaxial Tubes Filled With Incompressible Media: A Model of Pulse Transmission in the Intracranial Arteries," J. Fluids Struct., **16**(8), pp. 1029–1049.
[50] Elliott, N. S. J., Lockerby, D. A., and Broadbelt, A. R., 2009, "The Pathogenesis of Syringomyelia: A Re-Evaluation of the Elastic Jump Hypothesis," ASME J. Biomech. Eng., **131**, p. 044503.
[51] Bilston, L. E., Fletcher, D. F., and Stoodley, M. A., 2006, "Focal Spinal Arachnoiditis Increases Subarachnoid Space Pressure: A Computational Study," Clin. Biomech. (Bristol, Avon), **21**(6), pp. 579–584.
[52] Pillay, P. K., Awad, I. A., Little, J. R., and Hahn, J. F., 1991, "Symptomatic Chiari Malformation in Adults: A New Classification Based on Magnetic Resonance Imaging With Clinical and Prognostic Significance," Neurosurgery, **28**(5), pp. 639–645.
[53] Roosen, N., Dahlhaus, P., Lumenta, C. B., Lins, E., Stork, W., Gahlen, D., and

Bock, W. J., 1988, "Magnetic Resonance (MR) Imaging in the Management of Primary and Secondary Syringomyelic Cavities, and of Other Cystic Lesions of the Spinal Cord," Acta Neurochir. Suppl. (Wien), **93**, pp. 13–16.
[54] Zarzur, E., 1996, "Mechanical Properties of the Human Lumbar Dura Mater," Arq. Neuropsiquiatr., **54**(3), pp. 455–460.
[55] Patin, D. J., Eckstein, E. C., Harum, K., and Pallares, V. S., 1993, "Anatomic and Biomechanical Properties of Human Lumbar Dura Mater," Anesth. Analg. (Paris), **76**(3), pp. 535–540.
[56] Ozawa, H., Matsumoto, T., Ohashi, T., Sato, M., and Kokubun, S., 2004, "Mechanical Properties and Function of the Spinal Pia Mater," J. Neurosurg. Spine, **1**(1), pp. 122–127.
[57] Oakland, R. J., Hall, R. M., Wilcox, R. K., and Barton, D. C., 2006, "The Biomechanical Response of Spinal Cord Tissue to Uniaxial Loading," Proc. Inst. Mech. Eng., Part H: J. Eng. Med., **220**(4), pp. 489–492.
[58] Fiford, R. J., and Bilston, L. E., 2005, "The Mechanical Properties of Rat Spinal Cord In Vitro," J. Biomech., **38**(7), pp. 1509–1515.
[59] Gefen, A., and Margulies, S. S., 2004, "Are In Vivo and In Situ Brain Tissues Mechanically Similar?" J. Biomech., **37**(9), pp. 1339–1352.
[60] Bloomfield, I. G., Johnston, I. H., and Bilston, L. E., 1998, "Effects of Proteins, Blood Cells and Glucose on the Viscosity of Cerebrospinal Fluid," Pediatr. Neurosurg., **28**(5), pp. 246–251.
[61] Nakamura, M., Chiba, K., Nishizawa, T., Maruiwa, H., Matsumoto, M., and Toyama, Y., 2004, "Retrospective Study of Surgery-Related Outcomes in Patients With Syringomyelia Associated With Chiari I Malformation: Clinical Significance of Changes in the Size and Localization of Syrinx on Pain Relief," J. Neurosurg. Spine, **100**(3), pp. 241–244.
[62] Williams, B., 1970, "The Distending Force in the Production of Communicating Syringomyelia," Lancet, **296**(7662), pp. 41–42.
[63] Lichtor, T., Egofske, P., and Alperin, N., 2005, "Noncommunicating Cysts and Cerebrospinal Fluid Flow Dynamics in a Patient With a Chiari I Malformation and Syringomyelia—Part II," Spine, **30**(12), pp. 1466–1472.
[64] Greitz, D., Ericson, K., and Flodmark, O., 1999, "Pathogenesis and Mechanics of Spinal Cord Cyst. A New Hypothesis Based on Magnetic Resonance Studies of Cerbrospinal Fluid Dynamics," Int. J. Neuroradiology, **5**(2), pp. 61–78.
[65] Levy, E. I., Heiss, J. D., Kent, M. S., Riedel, C. J., and Oldfield, E. H., 2000, "Spinal Cord Swelling Preceding Syrinx Development. Case Report," J. Neurosurg., **92**(1), pp. 93–97.
[66] Ravaglia, S., Bogdanov, E. I., Pichiecchio, A., Bergamaschi, R., Moglia, A., and Mikhaylov, I. M., 2007, "Pathogenetic Role of Myelitis for Syringomyelia," Clin. Neurol. Neurosurg., **109**(6), pp. 541–546.
[67] Milhorat, T. H., Capocelli, A. L., Jr., Anzil, A. P., Kotzen, R. M., and Milhorat, R. H., 1995, "Pathological Basis of Spinal Cord Cavitation in Syringomyelia: Analysis of 105 Autopsy Cases," J. Neurosurg., **82**(5), pp. 802–812.
[68] Milhorat, T. H., 2000, "Classification of Syringomyelia," Neurosurg. Focus, **8**(3), pp. 1–6.
[69] Royo-Salvador, M. B., Sole-Llenas, J., Domenech, J. M., and Gonzalez-Adrio, R., 2005, "Results of the Section of the Filum Terminale in 20 Patients With Syringomyelia, Scoliosis and Chiari Malformation," Acta Neurochir., **147**, pp. 515–523.
[70] Sansur, C. A., Heiss, J. D., DeVroom, H. L., Eskioglu, E., Ennis, R., and Oldfield, E. H., 2003, "Pathophysiology of Headache Associated With Cough in Patients With Chiari I Malformation," J. Neurosurg., **98**(3), pp. 453–458.